SCIENTIFIC REPORTS

OPEN

Out-of-Plane Coordinated Porphyrin Nanotubes with Enhanced Singlet Oxygen Generation Efficiency

Qiang Zhao[1], Yao Wang[2], Yanshuang Xu[2], Yun Yan[1] & Jianbin Huang[1]

A supramolecular porphyrin nanotube displaying J-aggregation feature was constructed by out-of-plane coordinated bismuth-porphyrin. Significantly, compared to traditional J-aggregated porphyrin suffering from fluorescence and singlet oxygen quenching, the nanotube exhibits excellent bio-imaging ability and enhanced production efficiency of singlet oxygen. The out-of-plane structure of bismuth to porphyrin makes the aggregation an appropriate material for theranostics. Furthermore, it is also a potential radio-therapeutic drug owing to the presence of radio-active bismuth. Thus, the self-assembly of out-of-plane coordinated porphyrin can be a facile approach toward effective therapy of tumors and other diseases.
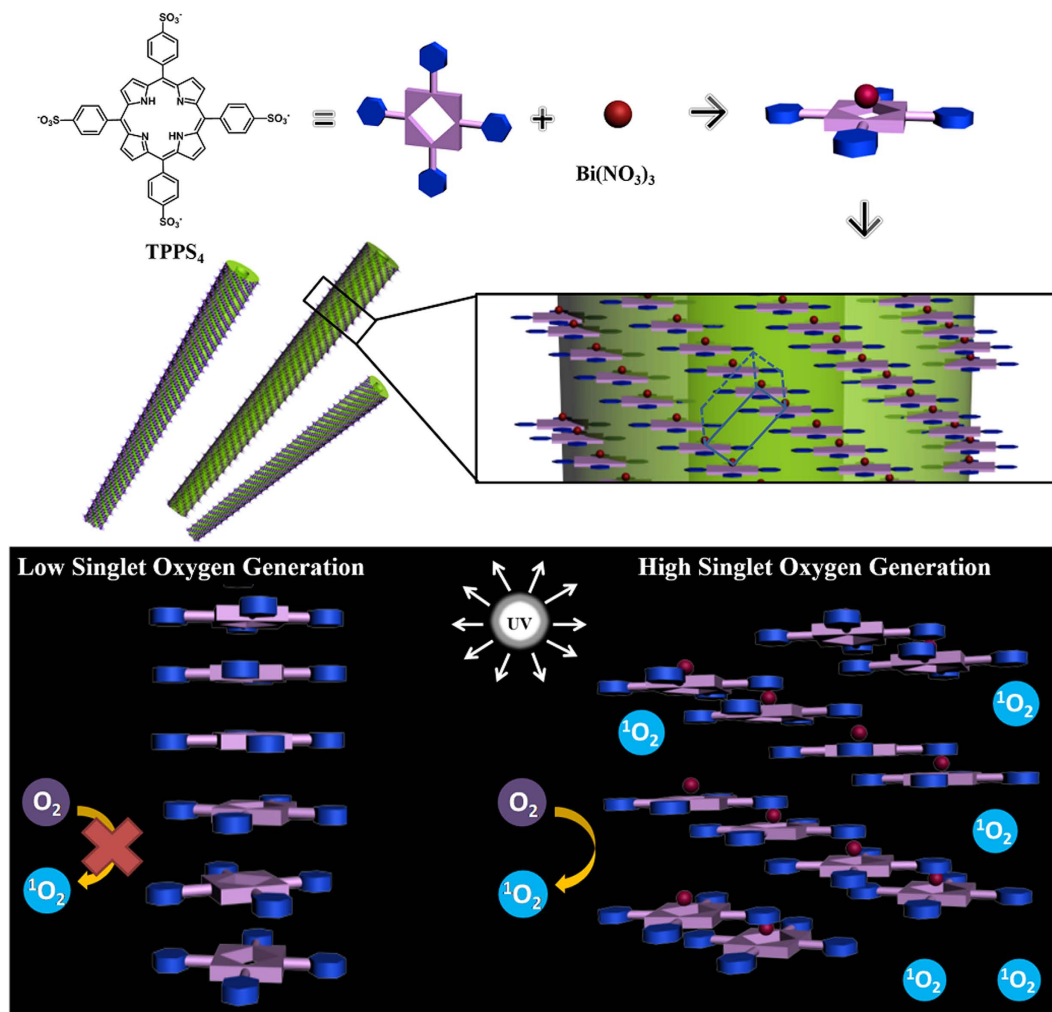
Photodynamic therapy (PDT) is a clinical method to eradicate early-stage cancer and to reduce the size of tumor in the end-stage cancer[1–3], which includes the combination of a photosensitizer, light and molecular oxygen ($^3O_2$)[4,5]. When exposed to the appropriate light, the photosensitizers can produce cytotoxic oxygen species leading to a selective and effective damage of diseased cells and tissues[6,7]. Hence, the photosensitizers with high singlet oxygen ($^1O_2$) quantum yield are desirable[8]. Porphyrins, as one of promising photosensitizers, have received much attention in PDT for their intense absorption and excellent singlet oxygen generation quantum yield[9]. Upon photo irradiation in UV-visible region, porphyrins transfer energy to triplet oxygen ($^3O_2$) and generate cytotoxic single oxygen ($^1O_2$) which causes cellular and tissue damage ultimately[10,11].

However, the large π-conjugate of planar porphyrin often undergoes obvious aggregation which causes severe quenching of the excited state thus leads to the decrease of $^1O_2$ generation[12,13]. It greatly limits the applications in biomedical field, especially in PDT application. To address this important issue, some space-demanding porphyrins have been introduced to segregate porphyrin units and suppress the quenching effect, such as co-assemble porphyrins with bulky molecules[14], load porphyrins to other nanostructures[15–17], and introduce steric moieties *via* organic synthesis[18–20], *etc*. In these processes, the strategies often involve complicated chemical synthesis, which is time-consuming and rises the risk of cytotoxicity due to the use of organic solvents. Therefore, pursuing a non-covalent method to make functional porphyrin nanostructures still remains challenging.

Metal porphyrins are known to facilitate the energy transfer *via* intersystem crossing[21,22], which is of key importance in the generation of singlet oxygen for PDT. Some metals coordinated with porphyrin and formed an out-of-plane structure that break the planar geometry and orderly arrangement of porphyrin[23–25]. Unfortunately, out-of-plane coordination can hardly drive well-defined porphyrin nanostructures so far. If the out-of-plane coordinated porphyrin can be employed properly, porphyrin nanostructures could be generated without close π-π stacking. It is of significant importance for suppressing the self-quenching in porphyrin aggregations and enhancing the efficiency of singlet oxygen generation.

Herein we report a rare case of J-aggregated porphyrin nanotubes with enhanced singlet oxygen generation efficiency. Tetrasodiummeso-tetra(sulfonatophenyl)porphine (TPPS$_4$) was employed to react with Bi(NO$_3$)$_3$ to generate TPPS$_4$-Bi nanotube. TPPS$_4$ is widely used as model porphyrins to study their self-assembling

[1]Beijing National Laboratory for Molecular Sciences (BNLMS), State Key Laboratory for Structural Chemistry of Unstable and Stable Species, College of Chemistry and Molecular Engineering, Peking University, Beijing 100871, People's Republic of China. [2]Beijing National Laboratory for Molecular Sciences (BNLMS), Key Laboratory of Polymer Chemistry and Physics of the Ministry of Education, College of Chemistry and Molecular Engineering, Peking University, Beijing 100871, People's Republic of China. Correspondence and requests for materials should be addressed to Y.Y. (email: yunyan@pku.edu.cn) or J.H. (email: jbhuang@pku.edu.cn)

Figure 1. Chemical structures of the TPPS$_4$ and the mechanism for the enhanced singlet oxygen efficiency of TPPS$_4$-Bi nanotubes compared with that of TPPS$_4$ aggregation.
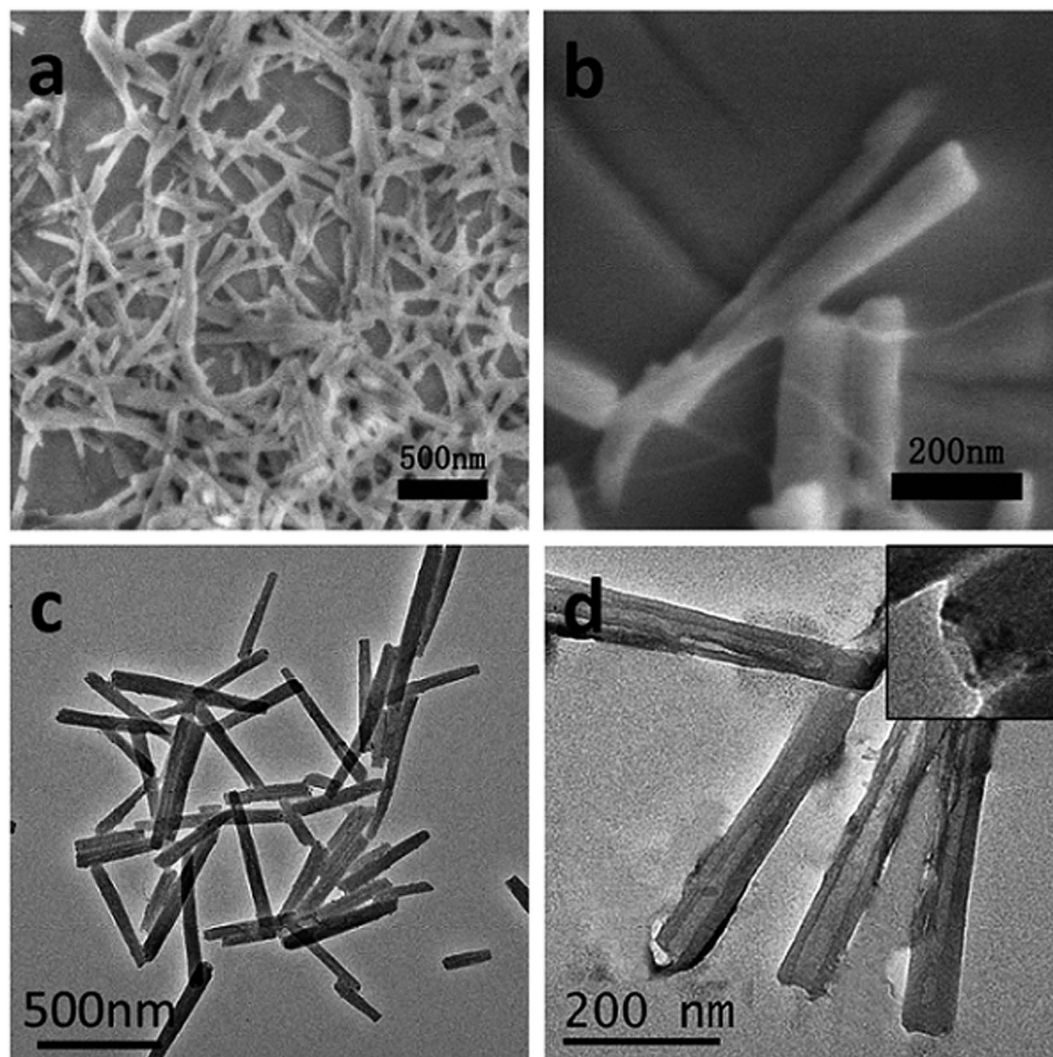
behaviors[26,27]. In this work, the TPPS$_4$ was found to self-assemble into nanotubes with Bi^{3+} by out-of-plane coordination. The coordination of Bi^{3+} makes a staggered arrangement of porphyrins so that it could reduce the overlap of porphyrin planar and suppress the self-quenching in aggregation (Fig. 1). Surprisingly, the nanotube exhibited an enhanced production of singlet oxygen similar to the monomeric porphyrins and an excellent fluorescence imaging ability in cells. Moreover, considering that Bi^{3+} also has wide applications in radio-therapy for the treatment of tumors and gastrointestinal disorders[28,29], the TPPS$_4$-Bi nanotube is expected to multiple functions as theranostics. The self-assembly of porphyrin which could suppress self-quenching without other co-assembling molecules or covalent modification is still challenging. Therefore, the present work opens a new vista to construct more porphyrin photosensitizers for the therapy of tumors and other diseases.
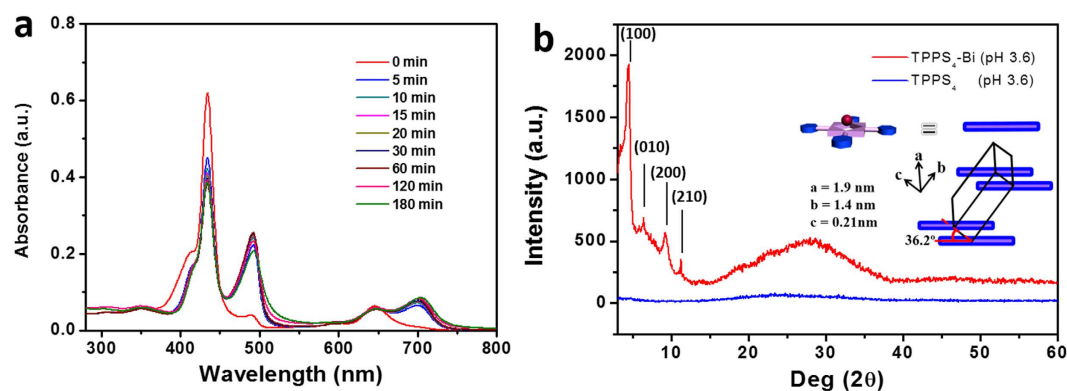
Results

The TPPS$_4$-Bi nanotube is fabricated in aqueous solution at pH 3.6, which is a condition that prohibits the hydrolysis of Bi^{3+}. In such acidic solution, TPPS$_4$ only could self-assemble into flexible and fiber-like J-aggregates which suspended in the solution (Supplementary Fig. S1)[30–33]. However, upon addition of Bi(NO$_3$)$_3$, precipitates were formed. TEM and SEM images demonstrate that the precipitates are composed of nanotubes with lengths and widths around 500 ± 100 nm and 50 ± 5 nm, respectively (Fig. 2). The wall-thickness of these nanotubes is only about 10–20 nm. EDX analysis reveals the presence of Na and Bi, suggesting these nanotubes are formed with TPPS$_4$ and Bi(NO$_3$)$_3$ (Supplementary Fig. S2).

Supramolecular structure of TPPS$_4$-Bi nanotubes was investigated using UV-Vis, fluorescence and circular dichroism (CD) spectroscopy. The TPPS$_4$ in aqueous solution displays two UV-Vis absorption bands at 434 and 645 nm. Upon addition of equimolar Bi^{3+}, these two bands gradually red shift to 491 and 707 nm, respectively, suggesting an increased extent of J-aggregation (Fig. 3a)[30–33]. Meanwhile, the fluorescence emission blue shifts from 680 nm to 516 nm, confirming that Bi^{3+} has induced further J-aggregation of TPPS$_4$ (Supplementary Fig. S3).

Figure 3b shows the X-ray diffraction (XRD) data for the TPPS$_4$-Bi nanotubes. Compared with J-aggregation of TPPS$_4$ only[30–33], sharp brag diffractions occur in TPPS$_4$-Bi nanotubes, suggesting Bi^{3+} has induced orthorhombic TPPS$_4$ crystal cells with a dimension of a = 1.9 nm, b = 1.4 nm, and c = 0.21 nm. It is noteworthy that

Figure 2. The SEM (**a,b**) and TEM (**c,d**) images of TPPS$_4$-Bi nanotubes. [TPPS$_4$] = 0.1 mM, [Bi^{3+}] = 0.2 mM, pH 3.6.

Figure 3. (**a**) Time dependent UV-Vis absorption of TPPS$_4$-Bi aqueous solution. [TPPS$_4$] = 0.025 mM, [Bi^{3+}] = 0.05 mM (pH 3.6). (**b**) XRD measurements for the TPPS$_4$-Bi nanotubes and TPPS$_4$ aggregates in acid aqueous solution (pH 3.6). The inset in (**b**) shows the arrangement of the TPPS$_4$ molecules in one cubic cell. The dislocation angle between the neighboring top and down TPPS$_4$ plane was 36.2°.

Bi^{3+} coordinates to TPPS$_4$ *via* out-of-plane coordination due to its large size with radius about 0.1 nm[23]. The distance between two neighboring TPPS$_4$ face is only 0.21 nm, much smaller than that of the 0.3 nm for the

	pH	τ/ns	Percentage of molecules with each lifetime (%)	Fitting quality χ^2
TPPS$_4$	6.8	11.75	84.03	0.9444
TPPS$_4$	3.6	3.783	94.13	1.062
TPPS$_4$-Bi	3.6	11.10	65.34	1.295

Table 1. The longest fluorescence lifetime (τ) of TPPS$_4$ under different conditions. The fraction of molecules with long lifetimes was given as hundred percent (%). The fitting quality was expressed by the parameter χ^2.

usual J-aggregated TPPS$_4$[25]. The electrostatic interactions between the Bi^{3+} of one TPPS$_4$ and the SO$_3^-$ of another one decrease distance between two TPPS$_4$ and result in the formation of the J-aggregated TPPS$_4$-Bi nanotubes. Based on the crystal cell parameters, the coordinated Bi^{3+} locates in between two dislocated TPPS4 planes and makes porphyrins arrange in a dislocation angle at about 36.2°, which is much smaller than the critical dislocation angle of 54.7° featuring J-aggregation[34]. As a result, the dislocation of porphyrin induces the stair-case type self-assembly of TPPS4 as illustrated in Fig. 1 and greatly reduces the extent of overlapping of porphyrin rings. In this way, the π-π stacking overlap was significantly reduced. Since the radius of Bi^{3+} is only around 0.1 nm which did not trigger extra steric hindrance for the arrangement of TPPS4, no induced chiral signal was observed upon formation of the nanotube (Supplementary Fig. S4). It is noticed that NO$_3^-$ could exist in nanostructure by coordination interaction between Bi and NO$_3^{-}$[35]. In addition, the TPPS$_4$-Bi nanotubes can be viewed as a nanostructure with 100% loading of porphyrins because no additional co-assembling molecules were added into the system.
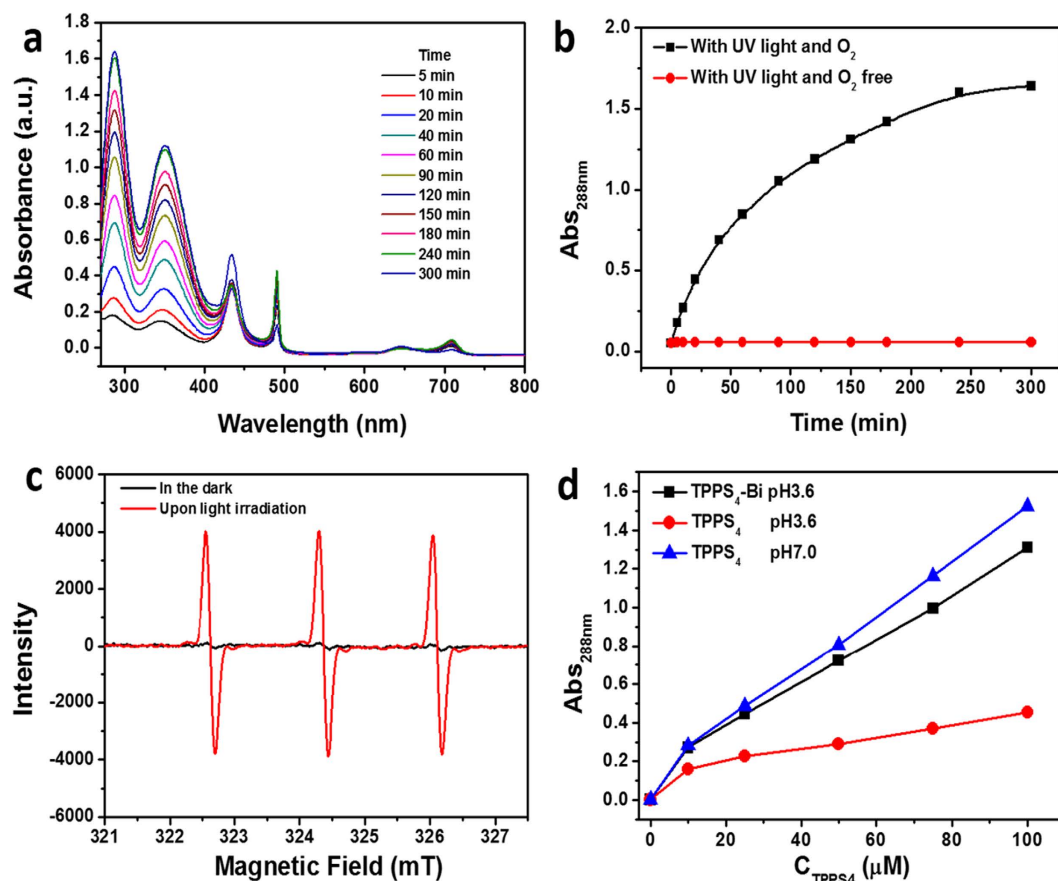
The suppression of self-quenching in TPPS$_4$-Bi was confirmed with time-resolved fluorescence studies (Supplementary Fig. S5 and Table 1). In neutral solution, 84% TPPS$_4$ exhibits a lifetime of 11.75 ns corresponding to the monomeric TPPS$_4$[36]. Before addition of Bi^{3+}, 94% porphyrin in J-aggregated TPPS$_4$ at pH 3.6 exhibits a short lifetime of 3.8 ns, which indicates that the π-π stacking overlap of TPPS$_4$ in J-aggregation have resulted in self-quenching of porphyrin. However, the lifetime is remarkably enhanced in J-aggregated TPPS$_4$-Bi system at pH 3.6, 65% TPPS$_4$ has the unprecedented long lifetime of about 11.10 ns, similar to that of monomeric TPPS$_4$ (Table 1). In addition, the long lifetime luminescence of TPPS$_4$-Bi corresponds with triplet stated that the emission at 600 nm could be quenched by oxygen[37], as shown in Supplementary Fig. S6. It is suggested that TPPS$_4$-Bi system possesses the potential in generation of singlet oxygen. The tubular structures and presence of heavy atom both promoted the intra-system crossing (ISC) which leads to the enhancement of photophysical properties.

The long lifetimes of porphyrin in TPPS$_4$-Bi system allow the nanotubes display excellent ability of singlet oxygen generation which was verified by iodide method and electron paramagnetic resonance (EPR) spectroscopy. The principle of this method is that the amount of I$_3^-$ produced by oxidation of I$^-$ with ^{1}O$_2$ is proportional to the concentration of ^{1}O$_2$ under continuous irradiation[38]. The light induced oxidation of iodide is chosen as model reactions for catalysis as Scheme S1. Figure 4a,b show that upon irradiation with UV light, the characteristic absorption of I$_3^-$ at λ = 350 nm and λ = 288 nm occurred, indicating the generation of ^{1}O$_2$ depending on time increasing. EPR spectroscopy was also employed to monitor the ^{1}O$_2$ generation ability of TPPS$_4$-Bi upon light irradiation. Trace amounts of 2,2,6,6-tetramethylpiperidine (TEMP), which is a diamagnetic and water-soluble molecule, was applied to capture ^{1}O$_2$ by yielding a paramagnetic product TEMPO[39,40]. The unpaired electron located on the NO group of TEMPO can lead to the hyperfine splitting of the EPR signal into three narrow lines, arising from the interaction between the unpaired electronic spin and the nitrogen nucleus. When the oxygen-saturated solution of TPPS$_4$-Bi was irradiated in the presence of TEMP for 10 min, the EPR signal increased as shown in Fig. 4c. The result of EPR test was in accordance with iodide method which confirmed the generation of singlet oxygen in TPPS$_4$-Bi system.

Moreover, compared with self-quenching J-aggregated TPPS$_4$ at pH 3.6, the TPPS$_4$-Bi nanotubes display a significantly enhanced singlet oxygen production (Fig. 4d). It is noteworthy that ability of singlet generation for TPPS$_4$-Bi nanotubes is comparable to that of monomeric porphyrins, which is probably benefited from the reduced π-π stacking by staggered porphyrin arrangement. Moreover, the nanotubes remain stable when dispersed in neutral water and the singlet oxygen generation ability was not apparently affected by changing pH (Supplementary Fig. S7). When the TPPS$_4$-Bi nanotubes were dispersed and irradiated by light in neutral solution or in oxygen free solution, there is no obvious generation of ^{1}O$_2$ (Figs 4b and S6).

The excellent singlet oxygen generation ability of the TPPS$_4$-Bi nanotube in neutral solution indicates a potential application in cells. We incubated the TPPS$_4$-Bi nanotubes with HeLa cell for 24 h. The cells are lighted up by the nanotube (Fig. 5a), and the strength of the green fluorescence is comparable to that of the commercial lysosome imaging dye Hoechst 33258 (Fig. 5b). The green and the blue window overlapped perfectly and resulted in the cyan fluorescence in the cell nucleus (Fig. 5c,d). Since the fluorescence of porphyrins is usually obtained as they exist in the isolated states, the present results indicate that the out-of-plane coordination have retained the monomeric porphyrin, which is in agreement with the detection of long lifetimes in time resolved fluorescence measurements.

The sufficient fluorescence of TPPS$_4$-Bi in HeLa cells manifests the possibilities of using this nanotube as theranostics, far beyond function solely as the PDT drug. Therefore, the PDT effect of the nanotube was tracked with its own fluorescence, rather than under the help of commercial dyes. Figure 5e,f are the images of the HeLa cells treated with 10 μM TPPS$_4$-Bi nanotubes before and after irradiation. Before irradiation, large amount of living cells are lighted up. In contrast, only several cells are observed after 10 min's irradiation followed by washing out the dead cells with water. A qualitative SRB analysis in Fig. 5g shows that half of the HeLa cells have been

Figure 4. Time depending (**a**) UV-Vis spectra of the TPPS$_4$-Bi nanotubes in the presence of KI and (**b**) the comparison of TPPS$_4$-Bi nanotubes in the presence of UV light and O$_2$ (□) and O$_2$ free (○), respectively. The absorption was at 288 nm. (**c**) EPR spectra of the TPPS$_4$-Bi nanotubes solution in which trace TEMP acts to capture the ^{1}O$_2$ generated in the dark or upon light irradiation for 10 min. (**d**) Compared singlet oxygen generation tested by UV-Vis spectra at $\lambda = 288$ nm with increasing concentrations at TPPS$_4$ (pH 7.0), TPPS$_4$ (pH 3.6) and TPPS$_4$-Bi (pH 3.6) systems. [TPPS$_4$] = 0.025 mM, [Bi^{3+}] = 0.05 mM, C$_{KI}$ = 1 M.

killed to death under the same condition. However, controlled experiments suggest that no cell death can be observed without irradiation. Meanwhile, blank test manifests that irradiation of untreated cells would not lead to considerable cell death, too (Supplementary Fig. S8), showing that the TPPS$_4$-Bi nanotubes display excellent phototoxicity.

In summary, we have prepared TPPS$_4$-Bi nanotubes through the facile out-of-plane coordination assisted self-assembly. The Bi^{3+} locates between two porphyrins at a dislocation angle which induces staggered arrangement of porphyrins and prevents π-π stacking overlap. It allows the TPPS$_4$-Bi J-aggregation to suppress the self-quenching effect and display an enhanced singlet oxygen generation compared with traditional TPPS$_4$ J-aggregation. Since the component Bi^{3+} is also a radio-therapy agent for tumors and other diseases, and there are judicious choices of functionally large metal ions and porphyrins, we expect that the out-of-plane coordination approach inspires much exciting design of porphyrin aggregations for multifunctional theranostics.
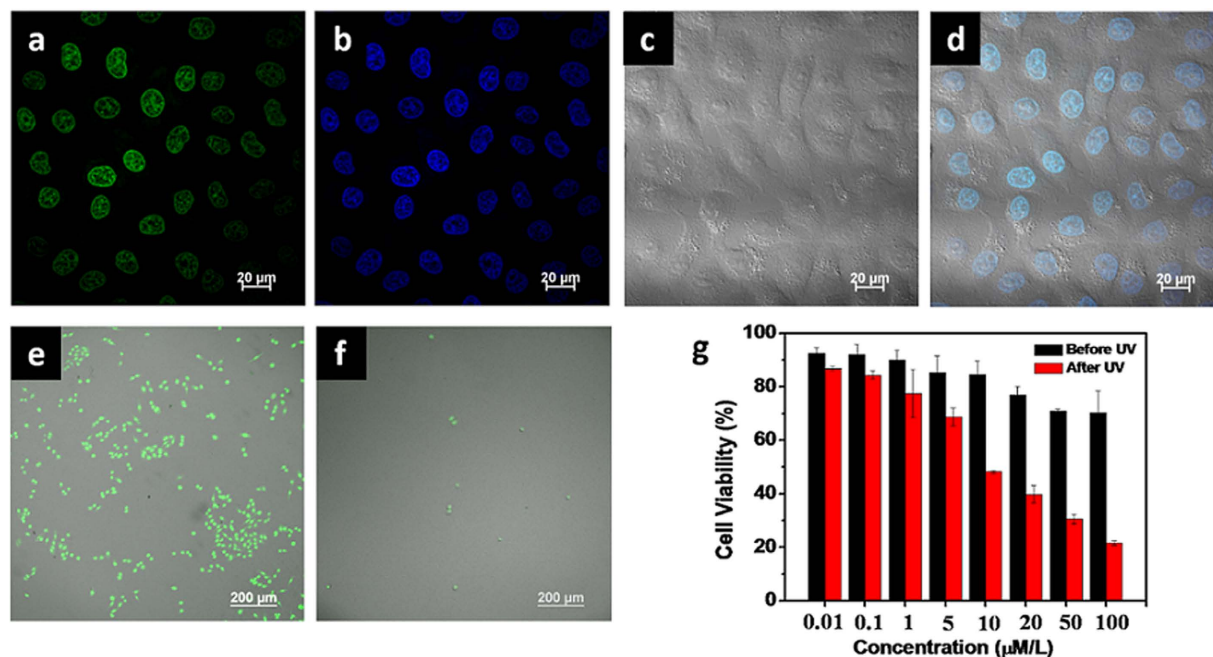
Methods

Materials. The tetrasodiummeso-tetra(sulfonatophenyl)porphine (TPPS$_4$, >97.0%) was purchased from Alfa Aesar. Bi(NO$_3$)$_3$·5H$_2$O, Zn(NO$_3$)$_3$, Pb(NO$_3$)$_3$ and TiCl$_4$ were purchased from Beijing Chemical Reagents (Beijing, China, >99.0%). All the aqueous solutions were prepared using Milli-Q water (Millipore, 18 MΩ/cm resistivity).

Preparation of TPPS$_4$-Bi Nanotubes. The porphyrin nanostructure were fabricated by mixing aqueous solutions of TPPS$_4$ and Bi(NO$_3$)$_3$ at pH 3.6. Typically, 0.1 mL of H$_4$TPPS$_4^{2-}$ solution (1 mM) was mixed with 0.2 mL of Bi(NO$_3$)$_3$ solution (1 mM) in 0.7 mL water, and the mixture as left undisturbed in the dark at 25 °C for 24 h. Over time, it provides a high yield of nanostructure.

Scanning Electron Microscopy (SEM). A drop of TPPS$_4$-Bi suspending solution was placed on clean silicon sheets and dried freely under ambient conditions. The samples were observed by a SEM, Hitachi S4800, 5 kV.

Transmission Electron Micrograph (TEM). Samples were observed by a Jeol JEM 100 CX, 80 kV and JEM-2100, 200 kV, together with energy-dispersive spectroscopy (EDS) measurement. Drops of samples were put

Figure 5. Confocal images of HeLa cells labeled with Hoechst 33258 after incubating with TPPS$_4$-Bi nanotubes. The fluorescent fields after (**a**) treated with 10μM mL^{-1} TPPS$_4$-Bi nanotubes and (**b**) Hoechst 33258 stained. (**c**) The optical field and (**d**) the overlap images of bright and fluorescence field in HeLa cells. The overlap images of bright field and fluorescence field (**e**) before and (**f**) after light irradiation in HeLa cells which were treated with 10μM mL^{-1} TPPS$_4$-Bi nanotubes. (**g**) SRB test for the cytotoxicity of TPPS$_4$-Bi nanotubes to HeLa cells after 48 hours incubation in various concentrations before and after UV irradiation. Data were presented as the mean $\pm$ standard deviation (N = 3).

onto 230 mesh copper grids coated with formvar film. Excess water was removed by filter paper and the samples were allowed to dry in ambient air at RT, before TEM observation. It is noticed that all samples were not stained except for the one which was made of TPPS$_4$ only.

Spectra Measurements. UV-Vis absorbance measurements were carried out on the Beijing Purkinje General Instrument Co. Ltd. TU-1810. The generation of singlet oxygen measured by UV-Vis absorption was carried out at 288 nm. The fluorescent measurements were tested by a fluorescent spectrophotometer, Hitachi F7000. The lifetime measurements of all samples were tested by a lifetime and steady state spectrometer (Edinburgh Instruments Ltd. FLS920). The circular dichroism (CD) spectrum was tested by a circular dichroism chiroptical spectrometer (Jasco Co.). All the spectra measurements were conducted at RT.

The light induced oxidation of iodide is chosen as model reaction for catalysis as previous reports. The reaction was shown in Scheme S1. The solution was deoxygen by nitrogen and kept in dark for 24 h. Before test, the solution was flowed by oxygen and added with KI. Then light was applied to induce the generation of ^{1}O$_2$. The ^{1}O$_2$ generation efficiency was tested by UV-Vis measurement at 288 nm absorption.

X-Ray Diffraction (XRD). For XRD measurements, several drops of suspension of TPPS$_4$ and TPPS$_4$-Bi were dropped on a clean glass slide respectively, followed by drying in the air. All samples were tested by an instrument (Rigaku Dmax-2000, Ni-filtered Cu Kα radiation) under ambient conditions at RT.

Singlet Oxygen Measurement. The EPR spectroscopy was used to monitor the generation of singlet oxygen in aqueous solutions. Singlet oxygen was detected as TEMP-^{1}O$_2$ adduct (TEMPO) using TEMP as a singlet oxygen trap. The EPR experiments were performed at room temperature on a JEOL JES-FA200 apparatus. The solution was saturated with oxygen, followed by addition of trace amount of TEMP and then irradiated by a xenon lamp with a sharp-cut filter (the cut off wavelength is 450 nm). The TEMPOL signal was analyzed by EPR.

Confocal Laser Scan Microscopy (CLSM). The samples were dropped on a clean glass slide and covered by a clean cover slip. A TCS-sp inverted confocal laser scanning microscope (Leica, Germany) was used to conduct experiments in florescence and differential interference contrast (DIC) modes.

Cell Culture and Cytotoxicity Assay *in Vitro*. In this study, HeLa cell lines were used. The HeLa cells (Institute of MateriaMedica, Chinese Academy of Medical Sciences and Peking Union Medical College, Beijing, China) were routinely grown in DMEM medium supplemented by 10% heated-inactivated fetal bovine serum (FBS), 100 U/mL penicillin and 100 mg/mL streptomycin. Cells were maintained at 37 °C with 5% CO$_2$. For cytotoxicity tests, HeLa cells were seeded into 96-well culture plates at a density of 5×10^3 cells/well and grown for 24 h. Then TPPS$_4$-Bi nanotubes were added into 96-well culture plates. The concentration of TPPS$_4$-Bi nanotubes

were in the range of $1 \times 10^{-3} - 50\,\mu M\,mL^{-1}$. Then after 48 h incubation, the cell viability was measured by a microplate reader at 540 nm with the SRB staining assay. The following formula was used: Survival% = (A_{540nm} for the treated cells/A_{540nm} for the control cells) × 100%, where the A_{540nm} was the absorbance value. Each assay was repeated for 5 times.

Confocal Microscopic Imaging of Cells Using TPPS$_4$-Bi Nanotubes. The HeLa cells were seeded into 96-well culture plates at a density of 5×10^3 cells/well and grown for 24 h. The cells were taken with $4\,\mu g\,mL^{-1}$ TPPS$_4$-Bi nanotubes for 4 h at 37 °C. Afterward, the cells were washed three times with PBS to remove the non-internalized nanotubes and incubated for another 24 h in a 24-well plate. Then the cells were fixed with 4% paraformaldehyde for 10 min and stained with $10\,\mu g\,mL^{-1}$ Hoechst 33258 at room temperature. Cell images were taken with a confocal laser scanning microscope with the excitation wavelengths of 405 nm and 488 nm.

References

1. Dolmans, D., Fukumura, D. & Jain, R. K. Photodynamic therapy for cancer. *Nat. Rev. Cancer* **3,** 380–387 (2003).
2. Bhaumik, J., Mittal, A. K., Banerjee, A., Chisti, Y. & Banerjee, U. C. Applications of phototheranostic nanoagents in photodynamic therapy. *Nano Res.* **8,** 1373–1394 (2015).
3. Castano, A. P., Mroz, P. & Hamblin, M. R. Photodynamic therapy and anti-tumour immunity. *Nat. Rev. Cancer* **6,** 535–545 (2006).
4. Hou, L., Zhang, X., Pijper, T. C., Browne, W. R. & Feringa, B. L. Reversible photochemical control of singlet oxygen generation using diarylethene photochromic switches. *J. Am. Chem. Soc.* **136,** 910–913 (2014).
5. Tian, J. *et al.* Cell-specific and pH-activatable rubyrin-loaded nanoparticles for highly selective near-infrared photodynamic therapy against cancer. *J. Am. Chem. Soc.* **135,** 18850–18858 (2013).
6. Moore, C. M., Pendse, D. & Emberton, M. Photodynamic therapy for prostate cancer-a review of current status and future promise. *Nat. Clin. Pract. Urol.* **6,** 18–30 (2009).
7. Tian, G., Zhang, X., Gu, Z. & Zhao, Y. Recent advances in upconversion nanoparticles-based multifunctional nanocomposites for combined cancer therapy. *Adv. Mat.* **27,** 7692–7712 (2015).
8. Ge, J. *et al.* A graphene quantum dot photodynamic therapy agent with high singlet oxygen generation. *Nat. Commun.* **5,** 1–8 (2014).
9. Singh, S. *et al.* Glycosylated porphyrins, phthalocyanines, and other porphyrinoids for diagnostics and therapeutics. *Chem. Rev.* **115,** 10261–10306 (2015).
10. Liu, M., Zhang, L. & Wang, T. Supramolecular chirality in self-assembled systems. *Chem. Rev.* **115,** 7304–7397 (2015).
11. Ethirajan, M., Chen, Y., Joshi, P. & Pandey, R. K. The role of porphyrin chemistry in tumor imaging and photodynamic therapy. *Chem. Soc. Rev.* **40,** 340–362 (2011).
12. Lovell, J. F. *et al.* Porphysome nanovesicles generated by porphyrin bilayers for use as multimodal biophotonic contrast agents. *Nat. Mat.* **10,** 324–332 (2011).
13. Jin, C. S., Lovell, J. F., Chen, J. & Zheng, G. Ablation of hypoxic tumors with dose-equivalent photothermal, but not photodynamic, therapy using a nanostructured porphyrin assembly. *ACS Nano* **7,** 2541–2550 (2013).
14. Liu, K. *et al.* Supramolecular photosensitizers with enhanced antibacterial efficiency. *Angew. Chem. Int. Edit.* **52,** 8285–8289 (2013).
15. Liu, T.-F. *et al.* Topology-guided design and syntheses of highly stable mesoporous porphyrinic zirconium metal-organic frameworks with high surface area. *J. Am. Chem. Soc.* **137,** 413–419 (2015).
16. Wilcox, O. T. *et al.* Acid loaded porphyrin-based metal-organic framework for ammonia uptake. *Chem. Commun.* **51,** 14989–14991 (2015).
17. Ding, Y., Tang, Y., Zhu, W. & Xie, Y. Fluorescent and colorimetric ion probes based on conjugated oligopyrroles. *Chem. Soc. Rev.* **44,** 1101–1112 (2015).
18. Chatterjee, D. K., Fong, L. S. & Zhang, Y. Nanoparticles in photodynamic therapy: An emerging paradigm. *Adv. Drug Delivery Rev.* **60,** 1627–1637 (2008).
19. Son, K. J. *et al.* Photosensitizing hollow nanocapsules for combination cancer therapy. *Angew. Chem. Int. Edit.* **50,** 11968–11971 (2011).
20. Liang, X., Li, X., Yue, X. & Dai, Z. Conjugation of porphyrin to nanohybrid cerasomes for photodynamic diagnosis and therapy of cancer. *Angew. Chem. Int. Edit.* **50,** 11622–11627 (2011).
21. Balaban, T. S., Tamiaki, H. & Holzwarth, A. R. Chlorins programmed for self-assembly. *Top. Curr. Chem.* **258,** 1–38 (2005).
22. Sengupta, S. & Würthner, F. Chlorophyll J-aggregates: From bioinspired dye stacks to nanotubes, liquid crystals, and biosupramolecular electronics. *Accounts Chem. Res.* **46,** 2498–2512, (2013).
23. Harvey, P. D. Reparameterized Herschbach-Laurie empirical relationships between metal-metal distances and force constants applied to homonuclear Bi- and polynuclear complexes (M = Cr, Mo, Rh, Pd, Ag, W, Re, Ir, Pt, Au, Hg). *Coordin. Chem. Rev.* **153,** 175–198 (1996).
24. Lemon, C. M., Brothers, P. J. & Boitrel, B. Porphyrin complexes of the period 6 main group and late transition metals. *Dalton T.* **40,** 6591–6609 (2011).
25. Preihs, C., Arambula, J. F., Lynch, V. M., Siddik, Z. H. & Sessler, J. L. Bismuth- and lead-texaphyrin complexes: towards potential alpha-core emitters for radiotherapy. *Chem. Commun.* **46,** 7900–7902 (2010).
26. Huang, C. *et al.* Ordered nanosphere alignment of porphyrin for the improvement of nonlinear optical properties. *Adv. Mat.* **22,** 3532–+ (2010).
27. Wang, Z. C., Medforth, C. J. & Shelnutt, J. A. Self-metallization of photocatalytic porphyrin nanotubes. *J. Am. Chem. Soc.* **126,** 16720–16721 (2004).
28. Briand, G. G. & Burford, N. Bismuth compounds and preparations with biological or medicinal relevance. *Chem. Rev.* **99,** 2601–2657 (1999).
29. Yang, N. & Sun, H. Biocoordination chemistry of bismuth: Recent advances. *Coordin. Chem. Rev.* **251,** 2354–2366 (2007).
30. Ribo, J. M., Crusats, J., Farrera, J. A. & Valero, M. L. Aggregation in water solutions of tetrasodium diprotonated meso-tetrakis(4-sulfonatophenyl)porphyrin. *J. Chem. Soc.-Chem. Commun.* 681–682 (1994).
31. Ohno, O., Kaizu, Y. & Kobayashi, H. J-Aggregate formation of a water-soluble porphyrin in acidic aqueous-media. *J. Chem. Phys.* **99,** 4128–4139 (1993).
32. Hasobe, T., Fukuzumi, S. & Kamat, P. V. Ordered assembly of protonated porphyrin driven by single-wall carbon nanotubes. J- and H-aggregates to nanorods. *J. Am. Chem. Soc.* **127,** 11884–11885 (2005).
33. Schwab, A. D. *et al.* Porphyrin nanorods. *J. Phys. Chem. B* **107,** 11339–11345 (2003).
34. Gandini, S. C. M., Gelamo, E. L., Itri, R. & Tabak, M. Small angle X-ray scattering study of meso-tetrakis (4-sulfonatophenyl) porphyrin in aqueous solution: A self-aggregation model. *Biophys. J.* **85,** 1259–1268 (2003).
35. Boitrel, B., Halime, Z., Balieu, S. & Lachkar, M. The coordination of bismuth by porphyrins. *C. R. Chimi.* **10,** 583–589 (2007).
36. Maiti, N. C., Mazumdar, S. & Periasamy, N. J- and H-aggregates of porphyrin-surfactant complexes: Time-resolved fluorescence and other spectroscopic studies. *J. Phys. Chem. B* **102,** 1528–1538 (1998).
37. Wilkinson, F., Helman, W. P. & Ross, A. B., Quantum yields for the photosensitized formation of the lowest electronically excited singlet-state of molecular-oxygen in solution. *J. Phys. Chem. Ref. Dat.* **22,** 113–262 (1993).

38. Mosinger, J. & Mosinger, B. Photodynamic sensitizers assay: Rapid and sensitive iodometric measurement. *Experientia* **51,** 106–109 (1995).
39. Moan, J. & Wold, E. Detection of singlet oxygen production by ESR. *Nature* **279,** 450–451 (1979).
40. Markovic, Z. *et al.* The mechanism of cell-damaging reactive oxygen generation by colloidal fullerenes. *Biomaterials* **28,** 5437–5448 (2007).

Acknowledgements

Author Contributions

Q.Z. performed all the experiments and involved in writing; Y.W. provided useful help in cell tests; Y.X. provided useful help in XRD tests; J.H. and Y.Y. proposed the study and revised the manuscript. All authors reviewed the manuscript.

Additional Information

Supplementary information accompanies this paper at http://www.nature.com/srep

Competing financial interests: The authors declare no competing financial interests.

How to cite this article: Zhao, Q. *et al.* Out-of-Plane Coordinated Porphyrin Nanotubes with Enhanced Singlet Oxygen Generation Efficiency. *Sci. Rep.* **6**, 31339; doi: 10.1038/srep31339 (2016).